Appl. Phys. B 86, 413–417 (2007)
DOI: 10.1007/s00340-006-2558-6

Applied Physics B
Lasers and Optics

R. GEHLHAAR✉
M. SWOBODA
M. SUDZIUS
M. HOFFMANN
H. FRÖB
V.G. LYSSENKO
K. LEO

Dual-wavelength laser emission from an organic microcavity with terahertz beating

Institut für Angewandte Photophysik, Technische Universität Dresden, 01062 Dresden, Germany

Received: 31 July 2006
Published online: 20 January 2007 •

ABSTRACT We report on the dynamics of laser emission from an anisotropic organic microcavity filled with the guest-host composite of tris-(8-hydroxy quinoline) aluminium (Alq_3) and 4-(dicyanomethylene)-2-methyl-6-(p-dimethylaminostyryl)-4H-pyran (DCM). In a single microcavity, a linesplitting of 0.18 THz between two perpendicularly polarized laser modes is observed. We ascribe this effect to an optical anisotropy in the distributed Bragg reflectors surrounding the organic layer. The temporal behavior of the electromagnetic field is studied by an up-conversion technique and shows an optical beating of 0.18 THz. Two modeling approaches are used to gain insight in the temporal evolution and phase behavior of the two modes. Both point towards the presence of a phase-coupling mechanism in this system.

PACS 42.55.Sa

1 Introduction

Vertical cavity surface emitting lasers (VCSELs) have attracted large interest in the past three decades [1]. Inorganic semiconductor VCSELs combine a very low threshold, high speed modulation capability and temperature insensitivity together with cheap module and packing costs. Cylindrical symmetric VCSELs offer an improved beam shape in comparison with edge emitting lasers that are combined with a disadvantageous competition between orthogonally polarized modes [2, 3]. Enhanced polarization stability is achieved by the introduction of an anisotropy within the system, e.g., by external strain [4], anisotropic geometry [5] or anisotropic oxide aperture [6].

The implementation of organic materials with their wide flexibility as an active medium in VCSELs provide different means of creating organic solid state lasers [7, 8]. Multimode emission from organic VCSELs with a controlled splitting in the terahertz range has not been reported previously. In addition, the phase properties of the individual modes were rarely studied. The comparably low fabrication costs of VCSELs offer a favorable way to create terahertz sources. If two modes are emitted with a frequency splitting in the terahertz range, this results in a beating, which could be used for terahertz difference signal generation. This would, however, require a coupled phase between two modes. Here, we present a VCSEL design with anisotropic mirrors, where two energetically shifted cross-polarized modes show a stable laser emission with a clearly defined phase relation.

✉ Fax: +49 351 463 370 65, E-mail: gehlhaar@iapp.de

2 Sample and experimental setup

The microcavity (cf. Fig. 1) consists of alternating $\lambda/4$-layers of TiO_2 and SiO_2, deposited by reactive electron beam evaporation on a glass substrate. These distributed Bragg reflectors (DBRs) surround an active medium of Alq_3 (tris-(8-hydroxy quinoline) aluminium) doped with 2% DCM (4-(dicyanomethylene)-2-methyl-6-(p-dimethylaminostyryl)-4H-pyran). The organic material is deposited by thermal coevaporation. The cavity layer thickness is ~ 650 nm, which corresponds to a distance of $3.7\lambda/2$ at the wavelength of observed laser emission. To achieve equal reflectance from both multilayer mirror structures, the DBR on the substrate side of the sample consists of 21 layers, while the top DBR consists of 19 layers. The design wavelength of the structure is 680 nm.

The inorganic layers are grown under an oblique deposition angle of about 15°, which leads to an anisotropic distribution of material on the substrate. Under these conditions, the dielectrics form columnar structures inclined at a certain angle with respect to the deposition angle [9, 10]. The column angle β is related to the deposition angle α by $\tan\alpha = 2\tan\beta$ [11, 12]. It has been established in both experiment [13, 14] and theory [15] that these columns lead to in-plane birefringence in the evaporated dielectric layers. Dielectric mirrors consisting of such anisotropic layers lead to the formation of two perpendicularly polarized cavity modes in microcavity structures [16]. Thus, by varying the deposition angle α, the spectral distance of the two modes can be tuned over a certain range.

We use the frequency-doubled output of a 1 kHz regenerative Ti:Sa amplifier to optically pump the organic microcavity. The up-conversion setup comprises a 200 μm nonlinear BBO crystal for sum-frequency mixing of the microcavity emis-

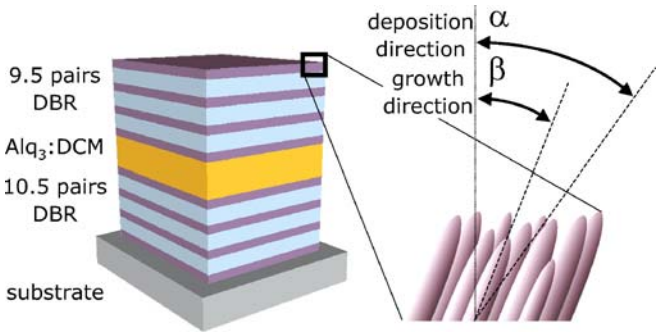

FIGURE 1 Structure of the organic VCSEL (left). The DBRs consist of alternating layers of SiO_2 and TiO_2 as low and high refractive index material, respectively. A columnar structure in the dielectric layers (right) leads to an optical anisotropy in the DBRs, thus creating two perpendicularly polarized emission modes. The column angle can be tuned by a variation of the deposition direction

sion with a 200 fs, 800 nm gate beam. The sum-frequency radiation is detected by a photomultiplier tube with 400 fs resolution. To record the emission spectrum, a 750 mm grating monochromator with charge coupled device (CCD) detector is used. The overall spectral resolution of the system is 0.023 nm.

3 Experimental results

3.1 *Spectrally resolved measurements*

The linear transmission spectrum of white light through the microcavity shows a narrow linewidth of $\Delta\lambda = 0.21$ nm for the cavity transmission mode, from which we estimate a quality factor Q of 2900. This corresponds by $Q = 2\pi c\tau_p/\lambda$ to a cavity photon lifetime τ_p of 0.95 ps.

Due to the in-plane anisotropy, polarization splitting is not only observed under a defined viewing angle as in previous reports [17, 18], but also at 0° [16].

The microcavity functions as an organic VCSEL [8, 19]. Pumping the sample with 400 nm radiation shows laser emission occurring at a threshold of 0.7 nJ pump pulse energy. We find two perpendicularly polarized laser modes at 612.46 nm and 612.69 nm, with ∼ 45 GHz and ∼ 40 GHz full width at half maximum (FWHM), respectively, which is on the order of the spectrometer resolution. The spectrum is shown in Fig. 2, with an apparent line splitting of 180.6 GHz between both emission modes.

3.2 *Light up-conversion results*

The temporal behavior of laser emission from the organic VCSEL is studied by a light up-conversion technique. The gate pulse of 200 fs defines a temporal resolution of 400 fs, which is sufficiently short to be neglected. The emitted laser pulses have pulse lengths between 5 ps and 50 ps dependent on the pump pulse energy [19]. This behavior is expected for the lasing in the single mode and is shown in Fig. 3. Here, the single mode case corresponds to one specific plane of polarization (cf. Fig. 2), where only the signal of one of the two modes is detected. The contribution of the modes to the upconversion signal can be tuned by means of a $\lambda/2$-plate.

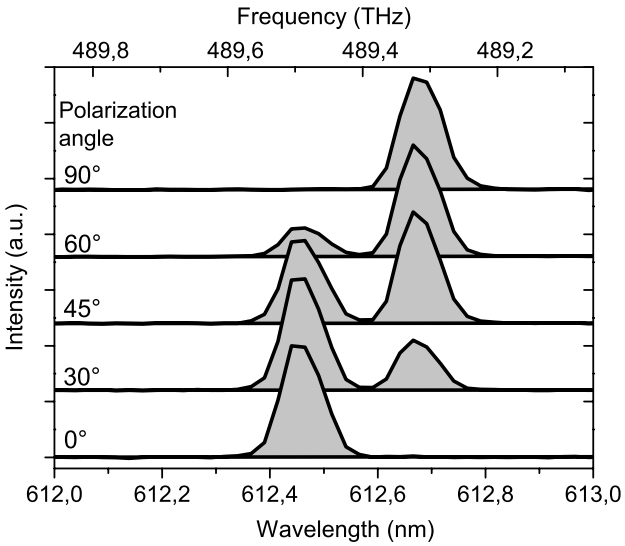

FIGURE 2 Normalized microcavity laser emission spectra in dependence of the polarizer angle. Two laser lines are observed, with either maximum at 90° and 0°

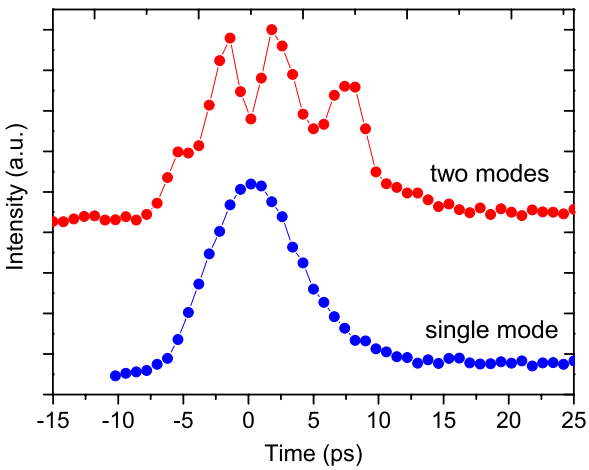

FIGURE 3 Experimental up-conversion results with two laser modes (*top*) contributing to the up-conversion signal with clearly visible interference oscillation at 5.5 ps period time, and with one mode (*bottom*). Each dot represents a single up-conversion measurement over several thousand pulses

In case the polarization plane is inclined by 45°, both modes contribute efficiently to the up-conversion signal. Figure 3 depicts the emission behavior at 45° polarization, when the two modes from the microcavity interfere to show a beating at 0.18 THz. For the polarization interference observed here, the beating frequency corresponds to the frequency splitting of the two initial modes. For a splitting of $\Delta\lambda = 0.23$ nm, an oscillation frequency of 180 GHz follows.

All the experimental data are obtained from averaging over many pulses. Thus, the interference phenomena that do not average out are observed. This implies that the phases of both modes are reproducibly coupled. As they are perpendicularly polarized, there should be no means of interacting or influencing their mutual phases. For an arbitrary mutual phase in each pumping cycle, the averaged signal should look like the single mode signal. This suggests a mode-coupling mechanism, which will be addressed in Sect. 4.2. It is, however, a crucial requirement in our following modeling approaches.

4 Modeling

4.1 *Rate equation modeling*

Rate equations provide an intuitive approach to understand lasing dynamics. They have been applied earlier to the present system [19, 20]. These equations describe the evolution of the excited molecules of the optically pumped system and the resulting photon numbers in the laser mode. With a suitable set of parameters, the up-conversion signal can be accurately reproduced. The laser pulse length is found to be mainly defined by the pump intensity. With increasing intensity, pulses as short as 5 ps can be generated. Close to the lasing threshold, the pulse length is about one order of magnitude larger. Also, the pump intensity defines the delay of the laser pulse peak intensity with respect to the pump pulse. Here, higher pump intensity means earlier pulse arrival at higher peak intensities.

With a description of the laser intensity dynamics, the resulting electric field can be obtained. In our case, we also account for the existence of two perpendicularly polarized lasing modes. The sum-frequency generation process is polarization selective and scales with electric field strength. Thus, we reconstruct the electrical field within the system as

$$E(t) = \sum_{m=1}^{2} \sqrt{I(t)} A_m \cos\theta_m \mathrm{e}^{\mathrm{i}(\omega_m t + \varphi_m)}\,, \tag{1}$$

where ω_m is the mode angular frequency, θ_m is the angle of the mode electric field with respect to the polarization plane of observation and $I(t)$ is the photon number function obtained from the rate equation approach. The angle θ_m accounts for the oscillation contrast. With $\theta_1 = \theta_2 + 90°$, we obtain maximum contrast at $\theta_1 = -\theta_2 = 45°$. A_m is an amplitude factor. In our calculations, we consider A_2 and φ_2 as fit parameters and set $A_1 = 1, \varphi_1 = 0$. Mode wavelength and splitting frequency are taken from the laser emission spectrum in Fig. 2. Spectrum and fitting procedure yield $A_2 = 0.2$, $\varphi_2 = 0$, $\hbar\omega_1 = 2024.37$ meV ($\lambda_1 = 612.46$ nm), $\hbar\omega_2 = 2023.62$ meV ($\lambda_2 = 612.69$ nm). The amplitude square of the resulting electric field is plotted in Fig. 4.

In the rate equation approach, the experimental results are reasonably reproduced. Oscillation frequency and pulse length can be derived. For phase and oscillation contrast, however, a number of assumptions are necessary, which will be addressed with a different approach in the next section.

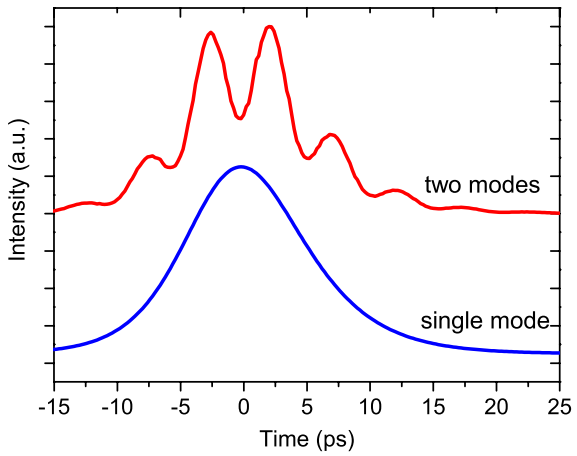

FIGURE 4 Results of rate equation based model for one (*bottom*) and two (*top*) contributing laser modes to the up-conversion signal

4.2 *Fourier transform approach*

As the phase behavior in the rate equation approach was a fitting parameter and thus postulated, we will now address the phase properties with a transfer matrix algorithm.

The transfer matrix method is a standard algorithm for optical thin film simulations [21]. It only allows one to calculate transmission and reflection, whereas emission properties cannot be taken into account easily. The cavity structure creates a phase shift of $\sim\pi$ at the cavity mode wavelength in transmission, whereas the phase of light that is transmitted through a single DBR is barely affected [22]. Therefore, this incoming light is assumed to be equal in phase to the light emitted inside the cavity. This assumption is supported by calculations of the emitted light phase based on the plane-wave expansion method [23, 24]. The combination of two mirrors and a cavity layer influences the phase properties of emitted and transmitted light in approximately the same way.

For the simulation of our anisotropic cavity, we use two structures with same layer thicknesses but different refractive indices for the DBR-layers. The layer sequence is shown in Fig. 1. In the model, the light source is situated at the substrate-DBR border and the transmitted phase is calculated for the DBR-air interface. The dispersion of the optical constants is neglected. This is justified by the narrow spectral region of the laser emission. For dielectric films evaporated at right angle, the optical constants were determined from ellipsometric measurements. We find for TiO_2 a real refractive index $n_{1,\mathrm{TiO_2}} = 2.17$ and an extinction coefficient $k_{1,\mathrm{TiO_2}} = 1 \times 10^{-4}$. For SiO_2, we determine $n_{1,\mathrm{SiO_2}} = 1.45$ and $k_{1,\mathrm{SiO_2}} = 2 \times 10^{-6}$. The design wavelength for the mirrors is chosen to be 680 nm and all DBR layer thicknesses are $\lambda/4$. The active layer of Alq_3 and DCM is modelled with the refractive index $n_{\mathrm{Alq_3}} = 1.72$ with the imaginary part $k_{\mathrm{Alq_3}} = 1 \times 10^{-4}$. The absorption-free substrate is modelled with $n_{\mathrm{Sub}} = 1.52$. To obtain a mode at 612.46 nm, an organic layer thickness of 655.49 nm is required. This layer thickness then represents approximately $3.7\lambda/2$.

To model perpendicular polarization, the refractive indices of the DBR layers are shifted such that the cavity mode is at 612.69 nm. As a further constraint, we keep the ratio of the two material refractive indices constant. This assumption is supported by considering the columnar growth of both materials as equal. The resulting values are $n_{2,\mathrm{TiO_2}} = 2.144$ and $n_{2,\mathrm{SiO_2}} = 1.432$.

The results for the transmission phases $\varphi_m(\omega)$ of each mode m are presented in Fig. 5b. The emission intensities $I_m(\omega)$ are obtained from the measured emission spectrum (Fig. 2) and fitted with a Gaussian function (Fig. 5a). Their positions are $\lambda_1 = 612.46$ nm and $\lambda_2 = 612.69$ nm with an equal width (FWHM) of 0.08 nm and an maximum intensity ratio of 0.76.

Both fields with their corresponding phase can be added up as they are emitted at the same time with a defined phase relation. Having constructed an electric field including spectral

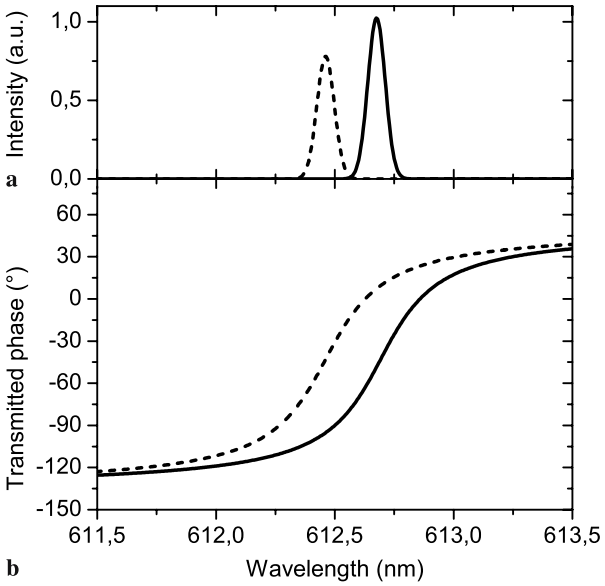

FIGURE 5 The fitted intensities (**a**) and the corresponding calculated phases (**b**) of the two emitted laser modes as used for the Fourier transform model. The two Gaussian lines represent the two emission modes. The phases of transmitted light for two microcavities with corresponding resonance frequencies. Around the resonance wavelength a phase shift of $\sim 150°$ occurs

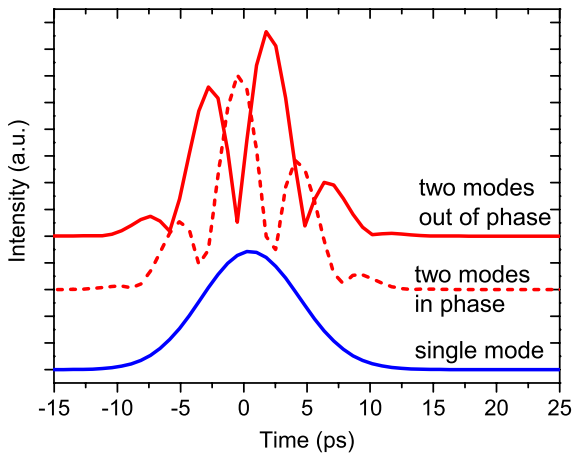

FIGURE 6 Fourier transform of one (*bottom*) and two contributing laser modes with Gaussian spectral shape. The temporal behavior shows a dependence on the initial phase relation. In the out of phase signal (*top*) the beating pulse with the maximum intensity occurs later than in the in phase transformation (*middle*)

phase allows one to then perform a Fourier transform

$$E(t) = \int_{-\infty}^{\infty} \sum_{m=1}^{2} \sqrt{I_m(\omega)} \mathrm{e}^{\mathrm{i}\varphi_m(\omega)} \mathrm{d}\omega \,, \tag{2}$$

to find the expected temporal behavior $E(t)$ of the system.

The results of the following Fourier transform are depicted in Fig. 6. The approach reproduces the characteristic occurrence of four major peaks at a periodicity corresponding to the spectral distance of the two peaks, with a Gaussian envelope with 11 ps duration. The results also show that it is indeed possible to model the cavity behavior with a Fourier transform approach based on the transmitted phase. However, the problem of the assumed phase relation of both peaks remains. Comparing Fig. 3 with Fig. 6, it is apparent that the better fit to the experimental data is obtained when assuming a fixed phase difference of $\Delta\varphi = \pi$ between both modes. This is explained, if we consider the existence of a mode-coupling mechanism, which will be addressed in the next paragraph.

The mode-coupling question is partly answered by phenomena in our anisotropic DBR mirrors. In accordance with coupled-mode theory [25], anisotropic media consisting of mutually detuned anisotropic layers can show coupling of perpendicularly polarized modes by repeated rotation of the mode polarization. The two modes exchange energy via the dielectric material response and an energy transfer occurs when a resonance phase-matching condition is met.

The fitting procedure in our model approaches shows equal phase for the rate equations and a π-phase difference between both modes in the Fourier approach. This discrepancy results from the inclusion of phase dispersion in the Fourier approach. A phase difference of $\Delta\varphi = 0$ would suggest that both modes stem from one initial event. A π-phase difference, however, agrees with the picture of mode-coupling via energy exchange in anisotropic media.

Due to energy exchange occurring between both modes, the onset of one will always result in the existence of the other mode, which is then amplified as well in the organic active layer after having left the mirrors again. First estimations of coupling strength and phase-matching for our system show that a finite energy transfer is indeed possible. Whether it is the cause of the phase-coupling process has not been verified at this point.

5 Conclusion

We have observed two perpendicularly polarized modes from a single cavity with anisotropic DBRs. The splitting between the two modes leads to a 0.18 THz beating seen in up-conversion of the emission. We deduce the existence of a phase-coupling mechanism in our system. The measurement results were modelled using two different approaches, both based on the assumption of present phase-coupling.

Our results seem promising for device applications due to the tunability of the beating frequency. In addition, the structure of only a single cavity offers a new way to produce light pulsing at terahertz frequencies based on photomixing techniques.

ACKNOWLEDGEMENTS The authors gratefully acknowledge funding by the EU Commission through 5th framework Research Training Network 'HYTEC' (HPRN-CT-2002-00315) and by the Deutsche Forschungsgemeinschaft via the Leibniz award.

REFERENCES

1 H. Li, K. Iga, *Vertical-Cavity Surface-Emitting Laser Devices* (Springer, Berlin, 2003), pp. 1–30
2 D. Burak, J.V. Moloney, R. Binder, Phys. Rev. A **61**, 053 809 (2000)
3 N.A. Loiko, I.V. Babushkin, J. Opt. B **3**, 234 (2001)
4 K. Panajotov, B. Nagler, G. Verschaffelt, A. Georgievski, H. Thienpont, J. Danckaert, I. Veretennicoff, Appl. Phys. Lett. **77**, 1590 (2000)
5 K.D. Choquette, R.E. Leibenguth, IEEE Photon. Technol. Lett. **6**, 40 (1994)
6 C.L. Chua, R.L. Thornton, D.W. Treat, R.M. Donaldson, Appl. Phys. Lett. **73**, 1631 (1998)

7 N. Tessler, G.J. Denton, R.H. Friend, Nature **382**, 695 (1996)
8 V. Bulovic, V.G. Kozlov, V.B. Khalfin, S.R. Forrest, Science **279**, 553 (1998)
9 Q. Tang, K. Kikuchi, S. Ogura, A. Macleod, J. Vac. Sci. Technol. A **17**, 3379 (1999)
10 G.K. Kiema, M.J. Colgan, M.J. Brett, Sol. Energ. Mater. Sol. Cells **85**, 321 (2005)
11 A.G. Dirks, H.J. Leamy, Thin Solid Films **47**, 219 (1977)
12 S. Lichter, J. Chen, Phys. Rev. Lett. **56**, 1396 (1986)
13 F. Flory, D. Endelema, E. Pelletier, I. Hodgkinson, Appl. Opt. **32**, 5649 (1993)
14 H. Wang, J. Phys. D Appl. Phys. **28**, 571 (1995)
15 H.A. Macleod, J. Vac. Sci. Technol. A **4**, 418 (1986)
16 R. Gehlhaar, M. Swoboda, M. Hoffmann, H. Fröb, V.G. Lyssenko, K. Leo, H. Wendrock, Appl. Phys. Lett. **88**, 091 121 (2006)
17 G. Panzarini, L.C. Andreani, A. Armitage, D. Baxter, M.S. Skolnick, V.N. Astratov, J.S. Roberts, A.V. Kavokin, M.R. Vladimirova, M.A. Kaliteevski, Phys. Rev. B **59**, 5082 (1999)
18 R. Gehlhaar, R. Schüppel, M. Koschorreck, T. Fritz, H. Fröb, M. Hoffmann, V.G. Lyssenko, K. Leo, L. Connolly, J. Wenus, D.G. Lidzey, J. Luminesc. **110**, 354 (2004)
19 M. Koschorreck, R. Gehlhaar, V.G. Lyssenko, M. Swoboda, M. Hoffmann, K. Leo, Appl. Phys. Lett. **87**, 181 108 (2005)
20 M. Swoboda, R. Gehlhaar, M. Sudzius, M. Hoffmann, H. Fröb, V.G. Lyssenko, K. Leo, Appl. Phys. Lett. **89**, 121 110 (2006)
21 H.A. Macleod, *Thin-Film Optical Filters* (Institute of Physics Publishing, Bristol, Philadelphia, 2001), 3rd Edn., pp. 12–85
22 P. Yeh, *Optical Waves in Layered Media* (John Wiley and Sons, Hoboken, NJ, 1988), p. 160
23 H. Benisty, H.D. Neve, C. Weisbuch, IEEE J. Quantum Electron. **QE-34**, 1612 (1998)
24 P. Royo, R.P. Stanley, M. Ilegems, IEEE J. Sel. Top. Quantum Electron. **8**, 207 (2002)
25 A. Yariv, P. Yeh, *Optical Waves in Crystals: Propagation and Control of Laser Radiation* (John Wiley and Sons, Hoboken, NJ, 2003), pp. 155–219